

A 60GHz LOS MIMO Backhaul Design Combining Spatial Multiplexing and Beamforming for a 100Gbps Throughput

Xiaohang Song*, Christoph Jans*, Lukas Landau*, Darko Cvetkovski† and Gerhard Fettweis*§

* Vodafone Chair, Technische Universität Dresden, Dresden, Germany,

Email: {xiaohang.song, christoph.jans, lukas.landau, fettweis}@tu-dresden.de

† Department of Computer Science, Humboldt Universität zu Berlin, Berlin, Germany,

Email: {darko.cvetkovski}@hu-berlin.de

Abstract—In this work, a two-level hierarchical MIMO system is proposed to combine the spatial multiplexing gain and beamforming gain in a strong LOS channel. The superior is a MIMO system that consists of specially arranged sub-arrays to fully exploit the spatial multiplexing gain in deterministic channels. Additionally, a deterministic spherical-wave channel model is introduced. This channel model includes the radiation patterns of the sub-arrays, orthogonal phase relations introduced by the specific sub-array arrangement and the path loss considering deployment in practical scenarios. The attenuation includes the free space path loss, the oxygen absorption, the rain attenuation in bad weather and the front-end loss. The regulations for the maximum radiated power and the available bandwidth at 60GHz were also investigated. Furthermore, the maximum transmission rate and upper bound of the energy efficiency are modeled and calculated for the proposed system operating at 60GHz compliant to those regulations, as well for a constraint of the maximum available transmit power on-board. The result shows that the proposed system architecture is promising to achieve over 100Gbps for macro-cell backhaul links with reasonable antenna sizes and high energy efficiency.

I. INTRODUCTION

One limit of utilizing millimeter waves (mm-W) in wireless communication is the high attenuation at this frequency range. Therefore designing antennas with high antenna gain is essential in overcoming the short range limitation. Applying beamforming on very densely packed antennas (referred to as sub-arrays in the latter sections) has been proved to provide high directivity and antenna gain in [1]. Accordingly, combining the high directivity antennas is required to cover enough distance and the spatial multiplexing from several of those high directivity antennas is promising to achieve very high data rates for applications like wireless backhaul.

The existing wireless backhaul solutions are realized using microwave dishes. However, each pair of dishes is only associated with one transmit link. For the macro-cell back-haul systems, line-of-sight (LOS) MIMO brings new challenges. Due to the almost stationary situation in wireless backhaul applications and high gain antennas with high directivity,

§ This work has been supported by the German Research Foundation (DFG) in the framework of the priority program SPP 1655 "Wireless Ultra High Data Rate Communication for Mobile Internet Access". The authors would like to thank Wolfgang Rave from TU Dresden and Eckhard Grass from Humboldt Universität zu Berlin, Germany for the valuable comments and feedback.

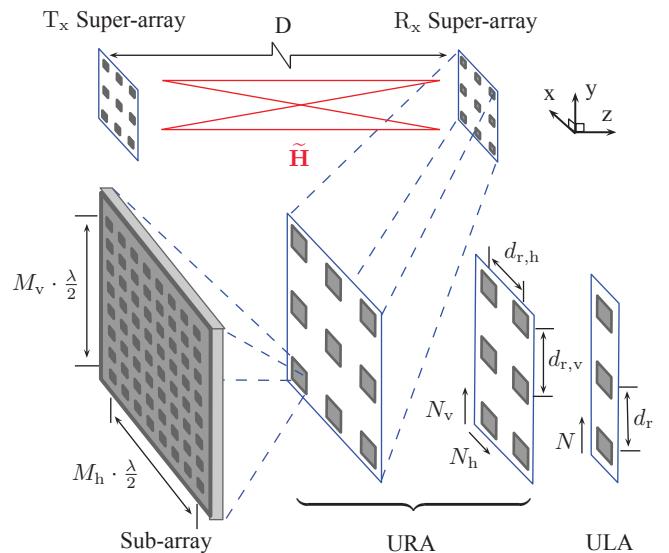


Fig. 1: A two-level hierarchical MIMO system with strong LOS channel model. The superior is a MIMO system that consists of $N = N_h \times N_v$ sub-arrays at each transceiver node.

we will use a *deterministic* MIMO channel model with sub-channels using the spherical-wave model. A recently published work [2] showed that, for strong LOS MIMO channels, the spherical-wave model is more accurate and optimistic than the conventional approach using plane-wave model. The specific geometry arrangements, like uniform linear arrays (ULA) and uniform rectangular arrays (URA), can fully exploit the spatial multiplexing gain in deterministic MIMO channel as reported in [3], [4], [5], [6]. The constructive interference from subchannels leads to deterministic channel matrices with approximate equal singular values.

In [4], [6], [7], [8], the authors have indicated that the antenna spacings mainly depend on the carrier wavelength λ , number of antenna elements N , and transmit distance D . The unlicensed large bandwidth at 60GHz brings a potential for developing ultra-high speed wireless backhaul communication systems with reasonable antenna sizes. For a practical system, the antenna aperture should be constrained to a certain space. For the parallel ULA, the optimal antenna spacing d_t and d_r

between sub-arrays at transmitter and receiver side given by [7], [8] satisfy

$$d_t \cdot d_r = \frac{\lambda D}{N}, \quad (1)$$

where the ULA consists of N antennas. Meanwhile, $d_{t,v}$, $d_{t,h}$ and $d_{r,v}$, $d_{r,h}$ for horizontal and vertical directions of the parallel URA given by [6] satisfy

$$d_{t,v} \cdot d_{r,v} = \frac{\lambda D}{N_v}, \quad d_{t,h} \cdot d_{r,h} = \frac{\lambda D}{N_h}, \quad (2)$$

where the transceivers consist of $N = N_v \times N_h$ antennas. According to Equation (2), a 4×4 MIMO system ($N = N_v \times N_h = 2 \times 2 = 4$) with symmetric transceivers at high carrier frequencies, such as 60GHz and a transmit distance of 100 meters is optimized with an antenna spacing 0.5m between sub-arrays.

The robustness of the capacity of strong LOS MIMO systems against errors like in-plane and out-of-plane translations and rotations has been well studied in [3], [4], [9], [10]. Meanwhile, the optimal antenna arrangements that compensate the tilt errors of the ULA and URA are studied by works in [7], [8] and [10] respectively. However, the work in [10] optimizes URA designs only for orientations across a single axis. As an extension, in [11] we introduce a method that optimizes antenna arrangements not only on tilted 2D planes but also on any arbitrary curved surfaces in a strong LOS MIMO channel, e.g. uniform parallelogram array on a plane with any tilt angle.

In this work, the parameters for designing a mm-W LOS MIMO system with a 100Gb/s transmission rate at 100m distance are evaluated. This includes a model for calculating the transmission rate and the energy efficiency. Furthermore, a calculation on the link budget shows there exists a trade-off between the number of sub-arrays and the number of antenna elements each sub-array should contain. Our investigations have been performed both accordingly to the Equivalent Isotropically Radiated Power (EIRP) regulations and a referenced the maximum transmit power that can be used in a practical system. One of the main advantages of our work is that all the computations are carried out based on a realistic channel model taking into account: free space path loss, oxygen absorption, rain attenuation, front end loss, element factor of identical antenna elements, array factor, thermal noise, noise figure, etc.

II. ANTENNA ARRAY DESIGN

We are considering a two-level hierarchical MIMO system with a strong LOS channel model as illustrated in Fig. 1. The superior is a MIMO system that contains $N = N_h \times N_v$ sub-arrays at each transceiver to fully exploit the spatial multiplexing gain in deterministic channels. The subordinate level refers to the architecture of the sub-arrays. As an example, all sub-arrays consist of $M_h \times M_v$ antenna elements with half wavelength spacing, $\lambda/2$. The transmit array (T_x) and the receive array (R_x) are facing each other and are arranged symmetrically. The direct links between each sub-array pair are the broadsides to the array planes.

The function of the sub-arrays is to provide a certain antenna gain and directivity of the transmission which makes the assumption of strong LOS channel more realistic in practical applications like LOS wireless backhaul. Considering analog beamsteering algorithms at a sub-array level, the system allows an acceptable compute complexity on higher level to fully exploit the spatial multiplexing gain.

As illustrated in Fig. 1, T_x and R_x are separated by D . The centroids of T_x and R_x are located at $(0, 0, 0)$ and $\mathbf{R}_0 = (0, 0, D)$ respectively. The coordinates of the phase center of j -th transmit sub-array and i -th receive sub-array are $\mathbf{t}_j = (x_j, y_j, 0)$ and $\mathbf{r}_i = \mathbf{R}_0 + \mathbf{t}_i$, $i, j \in [1, \dots, N]$, respectively. It is reasonable to assume that the distance D between T_x and R_x is much larger than the intra-array distances. Meanwhile, for simplicity, we neglect the inner-structure of the sub-arrays and we assume that intra-array distances are much larger than the inter antenna element distance. Consequently, we have $D \gg \|\mathbf{t}_i - \mathbf{t}_j\| \gg \lambda$.

However, as introduced by [3], [4], [9], [10], the ratio $\|\mathbf{t}_i - \mathbf{t}_j\|/\sqrt{\lambda \cdot D}$ has significant impacts on the channel characteristics and should not be a negligible value in order to maintain the optimal design characteristics as introduced by Equation (1), (2). Therefore, the distance D_{ij} between the sub-array pair (i, j) can be formulated as

$$\begin{aligned} D_{ij} &= \|\mathbf{r}_i - \mathbf{t}_j\| = \|\mathbf{R}_0 + \mathbf{t}_i - \mathbf{t}_j\| \\ &= \sqrt{D + \|\mathbf{t}_i - \mathbf{t}_j\|^2}. \end{aligned} \quad (3)$$

Applying a first order Taylor expansion to the square root and considering $\|\mathbf{t}_i - \mathbf{t}_j\| \ll D$, D_{ij} is approximated as

$$D_{ij} \approx D \cdot \left[1 + \frac{1}{2} \cdot \left(\frac{\|\mathbf{t}_i - \mathbf{t}_j\|}{D} \right)^2 \right]. \quad (4)$$

Considering the path loss ρ between sub-array pairs as a function of D_{ij} , we have

$$\rho(D_{ij}) \approx \rho(D), \quad (5)$$

where the approximation is applied with neglecting the components of orders more than two. Therefore, the differences between the attenuation factors among the sub-channels are omitted.

For a both time-flat and frequency-flat strong LOS link, the effective channel gain between equally polarized j -th transmit sub-array and i -th receive sub-array is modeled as

$$h_{ij}^{\text{eff}} \triangleq B_{R_x}(\theta'_{ij}, \phi'_{ij}) \cdot \rho(D) \cdot e^{-j \frac{2\pi}{\lambda} (D_{ij} - D)} \cdot B_{T_x}(\theta_{ij}, \phi_{ij}), \quad (6)$$

where the common phase term $e^{-j \frac{2\pi}{\lambda} D}$ is deducted due to the fact that it is not influencing the capacity. $B_{T_x}(\theta, \phi)$ and $B_{R_x}(\theta, \phi)$ stand for the sub-array gain at the transmit and receive sub-arrays respectively (also known as beam pattern).¹ The θ and ϕ stand for the azimuth and elevation

¹Here we assume that the values for $B_{T_x}(\theta_{ij}, \phi_{ij})$ and $B_{R_x}(\theta_{ij}, \phi_{ij})$ are real values. The assumption is made by considering that the phase pattern of the sub-array are calculated with respect to the phase center of the sub-array. Furthermore, in far-zone field, the phase differences of the same signal radiated from different antenna elements of individual sub-arrays cancel each other in the summation of array factor. Therefore, the radiation pattern does not introduce any phase differences in different directions (θ_{ij}, ϕ_{ij}) .

angle of the antenna radiation pattern as indicated by Fig. 2. Due to the symmetric arrangement of the transceivers, we have $B_{T_x}(\theta, \phi) = B_{R_x}(\theta, \phi)$. Meanwhile the (θ_{ij}, ϕ_{ij}) denotes (θ, ϕ) in direction from j -th transmit sub-array to i -th receive sub-array and $(\theta'_{ij}, \phi'_{ij})$ denotes for (θ, ϕ) of the i -th opposed sub-array at receiver side in direction from i -th receive sub-array to j -th transmit sub-array. Considering the symmetric arrangement of the system, $(\theta'_{ij}, \phi'_{ij})$ satisfies $\theta'_{ij} = \theta_{ij}$, $\phi'_{ij} = 2\pi - \phi_{ij}$.

After normalizing the radiation pattern with the maximum sub-array gain $B_{\max}^{T_x}$, $B_{\max}^{R_x}$ of the transmit and receive sub-arrays, one may write the received signal on the superior layer as

$$\begin{aligned} \mathbf{y} &= \underbrace{B_{\max}^{R_x} \cdot B_{\max}^{T_x} \cdot \rho(D) \cdot \sqrt{\frac{P_T}{N}}}_{\triangleq A_{\max}^{\text{sub}}} \cdot \underbrace{(\mathbf{B}_r \circ \mathbf{H} \circ \mathbf{B}_t)}_{\triangleq \tilde{\mathbf{H}}} \cdot \mathbf{x} + \mathbf{n} \\ &= A_{\max}^{\text{sub}} \cdot \tilde{\mathbf{H}} \cdot \mathbf{x} + \mathbf{n}, \end{aligned} \quad (7)$$

where (\circ) denotes the Hadamard product. $\mathbf{x} \in \mathbb{C}^{N \times 1}$ is the transmitted signal with unitary transmit power $E(||\mathbf{x}||^2) = 1$. P_T is the total transmit power that is available at the transmitter side. \mathbf{n} is the white complex Gaussian noise vector with $\mathbf{n} \sim \mathcal{CN}^{N \times 1}(0, P_n)$ and P_n is the noise power at each receive sub-array. \mathbf{B}_t , \mathbf{B}_r are the sub-array gains introduced by the normalized radiated patterns at the transmitter and receiver side with $(\mathbf{B}_t)_{ij} = B_{T_x}(\theta_{ij}, \phi_{ij})/B_{\max}^{T_x}$, $(\mathbf{B}_r)_{ij} = B_{R_x}(\theta'_{ij}, \phi'_{ij})/B_{\max}^{R_x}$. $\mathbf{H} \in \mathbb{C}^{N \times N}$ is the normalized channel matrix, which implies that each element h_{ij} in \mathbf{H} has unit channel gain with entities $h_{ij} \triangleq e^{-j\frac{2\pi}{\lambda}(D_{ij}-D)}$. By considering the approximation in Equation (4), the phase term in h_{ij} is significantly affected by the term $\frac{2\pi \cdot ||\mathbf{t}_i - \mathbf{t}_j||^2}{2\lambda D}$ which is significant important in having an orthogonal or almost orthogonal channel matrix. Furthermore, the average signal-to-noise ratio (SNR) is independent of \mathbf{H} . The $\tilde{\mathbf{H}}$ is defined as cubic normalized channel matrix. The scalar term A_{\max}^{sub} actually is the maximum element-link amplitude of the field one may achieve with maximum sub-array gains.

When assuming equal power transmission, the maximum achievable bandwidth efficiency of the MIMO transmission given by [12], [13] can be formulated as

$$\begin{aligned} C &= \log_2 \det \left[\mathbf{I}_N + \frac{(A_{\max}^{\text{sub}})^2}{\sigma_n^2} \tilde{\mathbf{H}} \tilde{\mathbf{H}}^H \right] \\ &= \log_2 \det \left[\mathbf{I}_N + \frac{[B_{\max}^{R_x} \cdot B_{\max}^{T_x} \cdot \rho(D)]^2 \cdot P_T}{NP_n} \tilde{\mathbf{H}} \tilde{\mathbf{H}}^H \right] \\ &= \log_2 \det \left[\mathbf{I}_N + \frac{\bar{\gamma}}{N} \tilde{\mathbf{H}} \tilde{\mathbf{H}}^H \right] \end{aligned} \quad (8)$$

where $(.)^H$ denotes the Hermitian transpose operator. $\bar{\gamma} \triangleq [B_{\max}^{R_x} \cdot B_{\max}^{T_x} \cdot \rho(D)]^2 \cdot P_T/P_n$ is a devised received SNR at each sub-array that assumes the maximum sub-array gains are applied to all element-links. This item is introduced to simplify the calculation of the received SNR in latter sections.

Considering that a practical system should be very compact, in the latter sections of this paper, we investigate fully orthogonal subchannel \mathbf{H} between each sub-array pair. The

uniform rectangular super-arrays provide a denser sub-array distribution compared to ULAs with the same number of sub-arrays, thus being more compact with respect to the antenna aperture. Therefore, for a given number of sub-arrays N , the number of sub-arrays in the horizontal and vertical directions N_h , N_v in the most compact design follows

$$\arg \min_{N_v \geq N_h} (N_v - N_h), \text{ s.t. } N = N_v \cdot N_h. \quad (9)$$

III. COMBINATION OF SPACIAL MULTIPLEXING AND BEAMFORMING

For a fixed targeting transmission rate, a trade-off between the number of antenna elements within a sub-array and the number of sub-arrays in the complete super-array is required to clarify the system design.

A. Radiation Pattern of Individual Sub-array

Due to the high path loss of wireless communication systems at 60GHz, sub-array gains at the transmitter and receiver sides are introduced to overcome the SNR degradation from the high path loss. The sub-array gain is formulated with the sub-arrays that are introduced in Section II. Considering the pattern multiplication for arrays of identical elements [14], the beam pattern or radiation pattern $B_p(\theta, \phi)$ of far-zone field is equal to the product of the element factor $EF_p(\theta, \phi)$ and the array factor $AF_p(\theta, \phi)$, while the transceiver indicator is $p \in \{T_x, R_x\}$. That is

$$B_p(\theta, \phi) = EF_p(\theta, \phi) \cdot AF_p(\theta, \phi). \quad (10)$$

Assuming that the major lobes of all the sub-arrays at transceivers are pointing in the transmit direction (z -direction), the array factor $AF_p(\theta, \phi)$ of a URA with $M_h \times M_v$ antenna elements given by [15] would be represented by

$$\psi_h = \frac{\pi}{\lambda} d_h \sin(\theta) \cos(\phi), \quad (11)$$

$$\psi_v = \frac{\pi}{\lambda} d_v \sin(\theta) \sin(\phi), \quad (12)$$

$$AF_p(\theta, \phi) = \frac{1}{\sqrt{M_h}} \frac{\sin(M_h \psi_h)}{\sin(\psi_h)} \frac{1}{\sqrt{M_v}} \frac{\sin(M_v \psi_v)}{\sin(\psi_v)}, \quad (13)$$

where d_h , d_v denote the antenna spacing in horizontal and vertical directions of the sub-arrays and $d_h = d_v = \lambda/2$. A typical radiation pattern for a *uniform rectangular sub-array* of $M_h \times M_v$ isotropic antenna elements (or a typical array factor of a $M_h \times M_v$ array) is shown in Fig. 2.

B. Link Budget and Energy Efficiency Upper Bound

Communication in the 60GHz region suffers from high atmospheric attenuation (e.g. oxygen absorption) and rain attenuation which must be considered for the link budget calculation. In order to overcome the high attenuation, the antenna gains at transceivers are essential to compensate the SNR degradation. The maximum power gain G_{\max}^p of the transmit and receive sub-arrays satisfies

$$G_{\max}^p \triangleq [B_{\max}^p]^2. \quad (14)$$

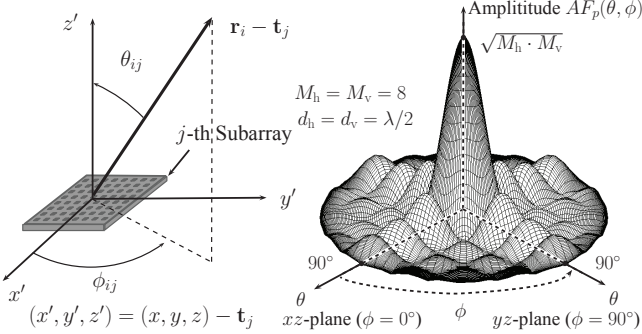


Fig. 2: Uniform Rectangular Sub-array Steering Vector Model.

The power attenuation $P_L(D) = \rho(D)^2$ in a strong LOS wireless channel can be formulated in [dB] as

$$P_L(D)[\text{dB}] \triangleq P_{\text{FE}}^{\text{T}_x}[\text{dB}] + P_{\text{fs}}(D)[\text{dB}] + P_{\text{oa}}(D)[\text{dB}] + P_{\text{ra}}(D)[\text{dB}] + P_{\text{FE}}^{\text{R}_x}[\text{dB}], \quad (15)$$

where the $P_{\text{fs}}(D)$, $P_{\text{oa}}(D)$, $P_{\text{ra}}(D)$, $P_{\text{FE}}^{\text{T}_x}$ and $P_{\text{FE}}^{\text{R}_x}$ are the free space path loss, oxygen absorption, the rain attenuation, front end loss of the T_x and R_x respectively. The free space path loss P_{fs} satisfies $P_{\text{fs}}(D) \triangleq (\frac{4\pi D}{\lambda})^2$ [16]. The noise power P_n in Equation (8) consists of the thermal noise P_{th} and the noise figure P_{nf} . The thermal noise P_{th} satisfies

$$P_{\text{th}}[\text{dBm}] \triangleq 10 \cdot \log_{10}(1000 \cdot k_B \cdot T \cdot W), \quad (16)$$

where k_B is the Boltzman constant ($k_B = 1.380649 \cdot 10^{-23} \text{ J/K}$), T is the absolute temperature in Kelvin and W is the allocated bandwidth. Based on the estimation of the path loss in Equation (15), the received SNR $\bar{\gamma}$ in Equation (8) can be calculated as

$$\bar{\gamma}[\text{dB}] = P_T[\text{dBm}] + G_{\max}^{\text{T}_x}[\text{dBi}] - P_L(D)[\text{dB}] + G_{\max}^{\text{R}_x}[\text{dBi}] - P_n[\text{dBm}], \quad (17)$$

where the P_T denotes transmit power. From Equation (8), the maximum achievable transmission rate R is given by

$$R = W \cdot C = W \cdot \log_2 \det(\mathbf{I}_N + \frac{\bar{\gamma}}{N} \tilde{\mathbf{H}} \tilde{\mathbf{H}}^H) \text{ bit/s.} \quad (18)$$

Furthermore, the upper bound of the energy efficiency as a function of M_h , M_v and N can be calculated as

$$\eta(M_h, M_v, N) \triangleq R/P_T \text{ bit/J.} \quad (19)$$

Due to the orthogonality of the \mathbf{H} matrix, the transmission rate scales with respect to the number of sub-arrays. In order to reduce the number of free parameters in the energy efficiency evaluation, we assume $M_h = M_v = M$. Furthermore, due to the fact that the ratio $\frac{R}{N \cdot P_T}$ barely varies with respect to N in later computation, we use the average value of upper bound of energy efficiency per sub-array over $N \in [1, N_{\max}]$ as the criteria to evaluate the energy efficiency, which as a function of M only is defined as

$$\bar{\eta}_n(M) \triangleq \frac{1}{N_{\max}} \sum_{N=1}^{N_{\max}} \frac{\eta(M, M, N)}{N} \text{ bit/J/Sub-array.} \quad (20)$$

IV. RESULT EVALUATION

For simplicity of the result evaluation and reducing the number of variables, we assume that each sub-array consist of $M_h \times M_v$ identically polarized antenna elements where $M_h = M_v = M$. The neighboring antenna elements are half the wavelength spaced in horizontal and vertical directions, $d_h = d_v = \lambda/2$. In order to build a robust MIMO system for the outdoor environment with a transmit distance of 100m, we assume operation under severe weather as the worst case scenario. As suggested by [17], in the given scenario, the values of the oxygen and rain attenuation $P_{\text{oa}}(D)$, $P_{\text{ra}}(D)$ at 60GHz would be approximately $P_{\text{oa}}(D) = 15 \text{ dB/km} \cdot D = 1.5 \text{ dB}$ and $P_{\text{ra}}(D) = 18 \text{ dB/km} \cdot D = 1.8 \text{ dB}$ (18dB/km for rainfall rate of 50mm/h), respectively. We assume a temperature of $T = 293 \text{ K}$ and a noise figure $P_{\text{nf}} = 5 \text{ dB}$, as typically it is in the range of 5 to 8dB.

Considering the proposed wireless backhaul system is operating at 60GHz, the 802.11ad standard defines that 'The transmit spectrum shall have 0dBm (dB relative to the maximum spectral density of the signal) bandwidth not exceeding 1.88GHz.' [18]. Therefore, the value for W is set as 1.88GHz.

In practice, the idea isotropic and point source antenna elements do not exist. Furthermore, the element factor $EF_p(\theta, \phi)$ depends on the design and the fabrication. Works in [19], [20], [21], [22], [23] focus on the dense packed sub-array design at 60GHz. A double-layer hollow-waveguide sub-array is proposed in [19]. The test antenna achieves about 8dBi/element with an efficiency of 80%. [20] focuses on the on-chip patch antennas design at 60GHz with 6.34dBi/element. However, the efficiency for CMOS patches have generally been low, about 14%. Studies have also been made for in-package patches with different materiel. [21] achieves 6dBi/element on fused silica. [22] achieves 7.4dBi/element with an efficiency of 60% on glass package substrate. [23] achieves 3 to 6dBi/element with estimated insertion loss of 2dB on LTCC. For simplicity, in the proceedings of the computation, we assume that $EF_p(\theta, \phi) = 6 \text{ dBi}$ and a front-end loss via assuming $P_{\text{FE}}^{\text{T}_x}[\text{dB}] = P_{\text{FE}}^{\text{R}_x}[\text{dB}] = 2 \text{ dB}$.

A. Result under EIRP Constraints

The EIRP limit regulates the emission to avoid harmful interference to authorized radio services in the band. The EIRP limit for 60GHz devices located outdoors has been amended to the following: 'The average EIRP limit from 40dBm to 82dBm minus 2dB for every dB that the antenna gain is below 51dBi' [24].² That means the EIRP limit $P_{\text{eirp}}[\text{dBm}]$ in terms of dBm for 60GHz devices located outdoors can be formulated as

$$P_{\text{eirp}}[\text{dBm}] \triangleq \max \left[\min \left[82 - 2(51 - G_{\max}^{\text{T}_x}[\text{dBi}]), 82 \right], 40 \right] \text{ dBm.} \quad (21)$$

²The peak EIRP limit is also amended with 3dBm addition to the average EIRP limit. For modulated signal with peak-to-average power ratio (PAPR) higher than 3dB, the maximal transmit power should be further restricted. In the proceedings of this paper, we neglect the possible degradation of the radiated power due to the high PAPR caused by the modulation schemes to provide an upper bound to the achievable transmission rate.

The maximum transmit power P_T that can be used is therefore constrained by the EIRP limit which includes the following components:

$$P_{\text{eirp}}[\text{dBm}] = P_T[\text{dBm}] + G_{\max}^{\text{T}_x}[\text{dBi}] - P_{\text{FE}}^{\text{T}_x}[\text{dB}]. \quad (22)$$

Considering the high demand for ever increasing transmission rates of the macro-cell backhaul in next generation communication systems, 100Gbps is a promising value for wireless backhaul links that replace the fiber backhaul links and further reduce the costs for fiber installation. Therefore, the computation, based on the model described above, focuses on link capacities higher than 100Gbps, as illustrated in Fig. 3.

The border of the none dark blue region in computation result shows that, for a fixed targeting transmission rate, there is a trade-off between M and N in system design. Furthermore, from Fig. 3, it can be found that the maximum date rate increases more rapidly with $M \geq 16$ due the fact that the sub-array gain is higher than 31dBi, which leads to an increment of the EIRP limit according to the regulations. If the antenna elements could provide higher element gain from the RF design, then requirement on M value can be further reduced and the performance of the system can be improved.

Considering the degradation of the system due to effects like RF impairments and possible high PAPR values, the system should be designed in a reasonable size with high date rate to provide some redundancy. Based on the Equation (2) and (18), the antenna size and the data rate under the optimal design are exemplified in Table I. For the system designs with indexes 1 to 4, it can be found that M has a significant impact on the SNR. However, for large M , the requirements for the RF chains might be too strong due to a high SNR. For the system designs with indexes 4 to 5 and 6 to 8, it can also be found that the capacity is almost linear with respect to N . We can conclude that at high SNR we would have a link capacity of $C \approx N \cdot C_{\text{SISO}}$ and that for arrays following the most compact design, the differences of the radiation patterns in targeting transmit directions are not very significant. Furthermore, the ratio $R/(N \cdot P_T)$ has a small variation and is insensitive to N .

The average energy efficiency per sub-array is illustrated in Fig. 4. It can be found that at region $M \leq 15$, the upper

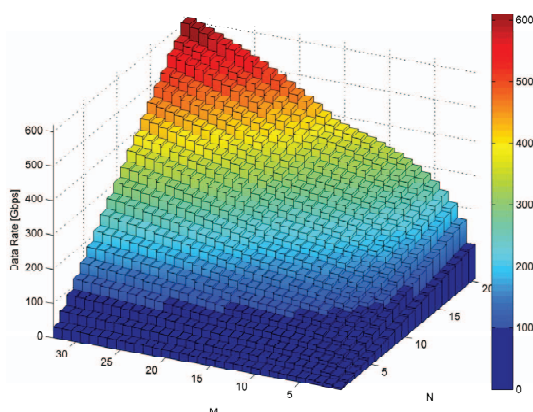


Fig. 3: Achievable Transmission Rates under EIPR Constraints.

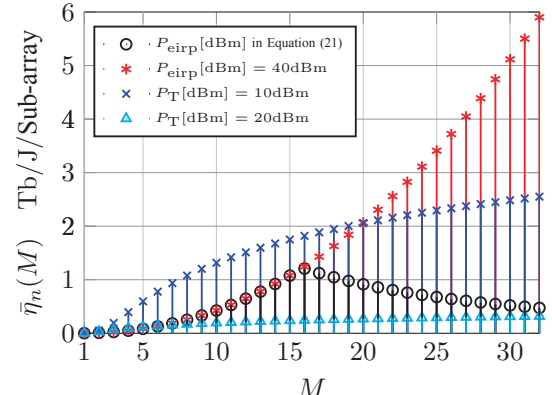


Fig. 4: Average over Upper Bound of Energy Efficiency Per Sub-array with $N_{\max} = 20$.

bound of the energy efficiency keeps creasing. In this region, the EIRP limit is a constant value. By increasing M , besides the increased transmission rate, the gain on energy efficiency is also obtained through the reduced transmit power. However, the energy efficiency gradually drops when $M \geq 16$ due to the fact that more transmit power is used. However, if the EIRP limit is a constant number, e.g. $P_{\text{eirp}} = 40\text{dBm}$ for indoor applications [24], the energy efficiency increases more rapidly as M increases.

B. Result under Maximum Transmit Power Constraints

As the backhaul applications are placed on roof-top, less harmful interference is created due to the spatial orthogonality and limit for human exposure only need to be considered in far-zone field. Although we are aware that the EIRP limits from the [24] has considered this effect for outdoor devices to encourage longer range 60GHz communication, for research purpose, the system performance under a maximum transmit power (regarding less of the EIRP limits) is also worth to be investigated. Furthermore, considering the cost for power amplifier (PA) at high output power is very high, it is typical to assume that, with a given PA, the maximum transmit power on-board is a constant number. Therefore, the computation result of link budget in Fig. 5 is made under assumption that $P_T[\text{dBm}] \leq 10\text{dBm}$ ($P_T \leq 10\text{mW}$).

From Fig. 5, the design of the system architecture can also

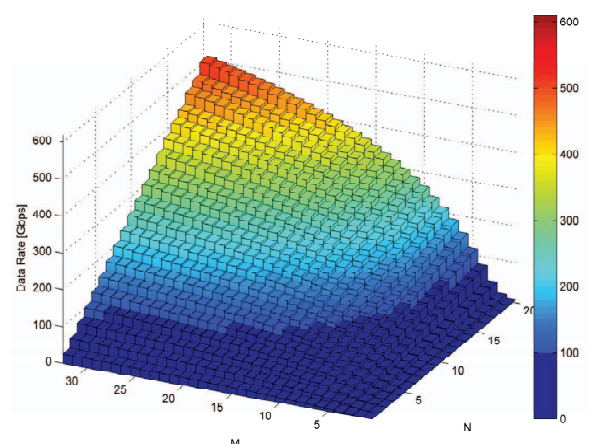


Fig. 5: Achievable Transmission Rates with $P_T \leq 10\text{dBm}$.

TABLE I: Example Parameters of Wireless Backhaul Systems under EIRP limit at a transmit Distance of 100m.

Index	$N = N_v \times N_h$	M^2	$R(\text{Gbps})$	$\bar{\gamma}[\text{dB}]$	$P_T[\text{dBm}]$	Height \times Width	Index	$N = N_v \times N_h$	M^2	$R(\text{Gbps})$	$\bar{\gamma}[\text{dB}]$	$P_T[\text{dBm}]$	Height \times Width
1	$4 = 2 \times 2$	23^2	101.7	40.8	15.2	0.50m \times 0.50m	5	$16 = 4 \times 4$	4^2	191.6	19.1	24.0	1.06m \times 1.06m
2	$6 = 3 \times 2$	10^2	101.4	27.1	16.0	0.82m \times 0.50m	6	$9 = 3 \times 3$	8^2	141.3	25.1	18.0	0.82m \times 0.82m
3	$8 = 4 \times 2$	5^2	105.4	21.1	22.0	1.06m \times 0.50m	7	$10 = 5 \times 2$	8^2	157.1	25.1	18.0	1.26m \times 0.50m
4	$9 = 3 \times 3$	4^2	107.8	19.1	24.0	0.82m \times 0.82m	8	$16 = 4 \times 4$	8^2	251.1	25.1	18.0	1.06m \times 1.06m

be evaluated for a fixed targeting transmission rate. The trade-off between M and N for a fixed targeting transmission rate still exists. The performance of the system does not outperform the link budget under EIRP limit due to the fact that the radiation power does not exceed the EIRP limit. However, by using better PA with higher P_T , e.g. $P_T[\text{dBm}] \leq 20\text{dBm}$, a higher transmission rate is expected when the radiated power is larger than EIRP limit. However, the energy efficiency, as one may expect, is lower as indicated in Fig. 4.

V. CONCLUSION

In this paper, we proposed a two-level hierarchical MIMO system that combines the spatial multiplexing gain and beamforming gain in a strong LOS channel intended for applications such as wireless backhaul. In addition to the system architecture, a realistic channel model together with models for calculating link budget and the upper bound of the energy efficiency are introduced. The realistic parameters for the proposed channel were plug-in for computations. The applied computations following IEEE 802.11ad and EIRP limit at 57-64GHz band regulations showed that the system is capable of achieving more than 100Gbps at a transmission distance of 100m with reasonable antenna sizes, especially for operation in the 60GHz band which exhibits high power attenuation. Meanwhile, the system designs under maximum transmit power on-board were also evaluated for a fixed targeting transmission rate and demonstrated. All results clearly showed that, for the system design targeting at a certain transmission rate, there exists a trade-off between the sub-array number and antenna element number in each sub-array. Meanwhile, the upper bounds of the energy efficiency following the above mentioned constraints were compared and showed a great potential in obtaining very high efficiency.

REFERENCES

- [1] J. Brady, N. Behdad, and A. Sayeed, "Beamspace MIMO for Millimeter-Wave Communications: System Architecture, Modeling, Analysis, and Measurements," *IEEE Transactions on Antennas and Propagation*, vol. 61, no. 7, pp. 3814–3827, 2013.
- [2] X. Pu, S. Shao, K. Deng, and Y. Tang, "Analysis of the Capacity Statistics for 2×2 3D MIMO Channels in Short-Range Communications," *IEEE Communications Letters*, vol. 19, no. 2, pp. 219–222, Feb 2015.
- [3] F. Bohagen, P. Orten, and G. Oien, "Design of Optimal High-Rank Line-of-Sight MIMO Channels," *IEEE Transactions on Wireless Communications*, vol. 6, no. 4, pp. 1420–1425, 2007.
- [4] P. Larsson, "Lattice Array Receiver and Sender for Spatially Orthogonal MIMO Communication," in *IEEE 61st Vehicular Technology Conference*, vol. 1, May 2005, pp. 192–196.
- [5] C. Sheldon, E. Torkildson, M. Seo, C. Yue, U. Madhow, and M. Rodwell, "A 60GHz Line-of-sight 2x2 MIMO Link Operating at 1.2Gbps," in *IEEE Antennas and Propagation Society International Symposium*, July 2008, pp. 1–4.
- [6] X. C. Chunhui Zhou, M. Z. Xiujun Zhang, Shidong Zhou, and J. Wang, "Antenna Array Design for LOS-MIMO and Gigabit Ethernet Switch-Based Gbps Radio System," *International Journal of Antennas and Propagation*, 2012.
- [7] D. Gesbert, H. Bolcskei, D. Gore, and A. Paulraj, "Outdoor mimo wireless channels: models and performance prediction," *IEEE Transactions on Communications*, vol. 50, no. 12, pp. 1926–1934, Dec 2002.
- [8] T. Haustein and U. Kruger, "Smart Geometrical Antenna Design Exploiting the LOS Component to Enhance a MIMO System Based on Rayleigh-fading in Indoor Scenarios," in *14th IEEE Proceedings on Personal, Indoor and Mobile Radio Communications*, vol. 2, Sept 2003, pp. 1144–1148.
- [9] F. Bohagen, P. Orten, and G. Oien, "Construction and Capacity Analysis of High-rank Line-of-sight MIMO Channels," in *IEEE Wireless Communications and Networking Conference*, vol. 1, March 2005, pp. 432–437.
- [10] ———, "Optimal Design of Uniform Planar Antenna Arrays for Strong Line-of-Sight MIMO Channels," in *IEEE 7th Workshop on Signal Processing Advances in Wireless Communications*, July 2006, pp. 1–5.
- [11] X. Song and G. Fettweis, "On Spatial Multiplexing of Strong Line-of-Sight MIMO with 3D Antenna Arrangements," *IEEE Wireless Communications Letters*, vol. PP, no. 99, pp. 1–1, 2015.
- [12] G. J. Foschini, "Layered Space-time Architecture for Wireless Communication in a Fading Environment when Using Multi-element Antennas," *Bell Labs Technical Journal*, vol. 1, no. 2, pp. 41–59, 1996.
- [13] E. Telatar, "Capacity of Multi-antenna Gaussian Channels," *European Transactions on Telecommunications*, vol. 10, no. 6, pp. 585–595, 1999.
- [14] C. A. Balanis, *Antenna Theory: Analysis and Design, 3rd Edition*. Wiley-Interscience, Apr. 2005.
- [15] H. L. V. Trees, *Detection, Estimation, and Modulation Theory, Optimum Array Processing*. New York: Wiley-Interscience; Part IV edition, 2002.
- [16] H. Friis, "A note on a simple transmission formula," *Proc. IRE*, vol. 34, p. 254, 1946.
- [17] P. F. M. Smulders and L. Correia, "Characterisation of Propagation in 60 GHz Radio Channels," *Electronics Communication Engineering Journal*, vol. 9, no. 2, pp. 73–80, Apr 1997.
- [18] "IEEE Standard for Information technology—Telecommunications and information exchange between systems—Local and metropolitan area networks—Specific requirements—Part 11: Wireless LAN Medium Access Control (MAC) and Physical Layer (PHY) Specifications Amendment 3: Enhancements for Very High Throughput in the 60 GHz Band," *IEEE Std 802.11ad-2012 (Amendment to IEEE Std 802.11-2012, as amended by IEEE Std 802.11ae-2012 and IEEE Std 802.11aa-2012)*, p. 443, Dec 2012.
- [19] Y. Miura, J. Hirokawa, M. Ando, Y. Shibuya, and G. Yoshida, "Double-layer full-corporate-feed hollow-waveguide slot array antenna in the 60-ghz band," *IEEE Transactions on Antennas and Propagation*, vol. 59, no. 8, pp. 2844–2851, Aug 2011.
- [20] H. Chu, Y. Guo, F. Lin, and X.-Q. Shi, "Wideband 60ghz on-chip antenna with an artificial magnetic conductor," in *IEEE International Symposium on Radio-Frequency Integration Technology, 2009. RFIT 2009*, Jan 2009, pp. 307–310.
- [21] D. Liu and R. Sirdeshmukh, "A patch array antenna for 60 ghz package applications," in *IEEE Antennas and Propagation Society International Symposium*, July 2008, pp. 1–4.
- [22] E. Herth, N. Rolland, and T. Lasri, "Circularly polarized millimeter-wave antenna using 0-level packaging," *IEEE Antennas and Wireless Propagation Letters*, vol. 9, pp. 934–937, 2010.
- [23] D. G. Kam, D. Liu, A. Natarajan, S. Reynolds, H.-C. Chen, and B. Floyd, "Ltc packages with embedded phased-array antennas for 60 ghz communications," *IEEE Microwave and Wireless Components Letters*, vol. 21, no. 3, pp. 142–144, March 2011.
- [24] F. C. Commission, "Part 15 of the Commissions Rules Regarding Operation in the 57-64 GHz Band, ET Docket No. 07-113 and RM-1104," August 2013.